Eur. Phys. J. C (2020) 80:600
https://doi.org/10.1140/epjc/s10052-020-8169-2

THE EUROPEAN PHYSICAL JOURNAL C

Regular Article - Theoretical Physics

Quasinormal modes of three-dimensional rotating Hořava AdS black hole and the approach to thermal equilibrium

Ramón Bécar[1,a], **P. A. González**[2,b], **Eleftherios Papantonopoulos**[3,c], **Yerko Vásquez**[4,d]

[1] Departamento de Ciencias Matemáticas y Físicas, Universidad Católica de Temuco, Montt 56, Casilla 15-D, Temuco, Chile
[2] Facultad de Ingeniería y Ciencias, Universidad Diego Portales, Avenida Ejército Libertador 441, Casilla 298-V, Santiago, Chile
[3] Department of Physics, National Technical University of Athens, Zografou Campus GR 157 73, 157 73 Athens, Greece
[4] Departamento de Física y Astronomía, Facultad de Ciencias, Universidad de La Serena, Avenida Cisternas 1200, La Serena, Chile

Received: 28 January 2020 / Accepted: 17 June 2020 / Published online: 2 July 2020

Abstract We compute the quasinormal modes (QNMs) of a massive scalar field in the background of a rotating three-dimensional Hořava AdS black hole, and we analyze the effect of the breaking of Lorentz invariance on the QNMs. Imposing on the horizon the requirements that there are only ingoing waves and at infinity the Dirichlet boundary conditions and the Neumann boundary condition hold, we calculate the oscillatory and the decay modes of the QNMs. We find that the propagation of the scalar field is stable in this background and employing the holographic principle we find the different times of the perturbed system to reach thermal equilibrium for the various branches of solutions.

1 Introduction

If a dynamical system is perturbed, it will return to equilibrium, and this process is completely determined by the poles of the retarded correlation function of the perturbation. In gravity theories, black holes are thermodynamical systems and perturbations of them at equilibrium are described by the quasinormal modes (QNMs) [1–7]. The QNMs are determined by solving the wave equation of an incident wave with the right boundary conditions. Then the solution of the wave equation determines the complex frequencies, the real part of which gives the rate of oscillations of the wave, while their complex part gives the required decay time for the system to reach thermal equilibrium.

The QNMs and quasinormal frequencies (QNFs) have been subjects of study for a long time and have recently acquired great interest due to the detection of gravitational waves [8]. Despite the detected signal being consistent with the Einstein gravity [9], there are great uncertainties in the mass and angular momenta of the ringing black hole, which leaves open possibilities for alternative theories of gravity [10] like $f(R)$ gravity [11–13] and Galileon gravity theories [14–16]. Also, the QNMs and the QNFs were extensively studied in connection with the stability of black holes in Einstein gravity [17–19] and in modified gravity theories [20–22].

The gauge/gravity duality which results from the AdS/CFT correspondence [23,25] stimulated the interest in calculating the QNMs and QNFs of black holes in AdS spacetime. It was shown in [26] that this holographic principle leads to the existence of a correspondence between the QNMs in AdS black holes and linear response theory in scale invariant finite temperature field theory. This correspondence of the decay of perturbations in the dual conformal field theory and the QNMs in the gravity bulk was first discussed in [27]. Considering the $(2+1)$-dimensional AdS black hole [28], it was shown analytically [26] that there is agreement between its QNFs and the location of the poles of the retarded correlation function describing the linear response on the conformal field theory side.

In this work we will consider a matter distribution in the background of three-dimensional rotating Hořava AdS black holes [29], parameterized by a scalar field. We will perturb the scalar field assuming that there is no back reaction on the metric. This will result in the calculation of the QNMs, which are characterized by a spectrum that is independent of the initial conditions of the perturbation and depends only on the black hole and probe field parameters, and on the fundamental constants of the system (for a review see [30]). It is worth mentioning that other black hole solutions in gravitational theories with broken Lorentz invariance have

[a] e-mail: rbecar@uct.cl
[b] e-mail: pablo.gonzalez@udp.cl
[c] e-mail: lpapa@central.ntua.gr
[d] e-mail: yvasquez@userena.cl (corresponding author)

been found; for instance, static and stationary exact solutions of the full theory of the projectable Hořava gravity with an extra $U(1)$ symmetry in $(2+1)$-dimensions, which is power-counting renormalizable [31]. Also, solutions for QNMs of black holes in three spacetime dimensions have been obtained in [32,33,35–42].

The motivation for considering the Hořava gravity theory is twofold. Considering a condensed matter dynamical system, it was argued in [43] that this condensed matter system breaks Lorentz invariance spontaneously and its excitations, the superfluid's phonons, have to non-linearly realize the spontaneously broken Lorentz boosts, forcing their interactions to have a very constrained structure. Then, to holographically describe such a system on the boundary, we need to have a broken Lorentz gravity theory in the bulk. The other motivation is, by calculating the QNMs, to see what is the effect of Lorentz breaking symmetry on the relaxation time of the dynamical system to reach thermal equilibrium on the boundary [44].

In this context, the QNMs for four-dimensional non-reduced Einstein-aether theory was studied, and it was found in [45] that the oscillation and damping rate of QNMs are larger than those of Schwarszschild black holes of the Einstein theory, for an effective potential that is known only numerically. More recently, the QNMs for two kinds of aether black holes were analyzed, and it was shown that quasinormal ringing of the first kind of aether black hole is similar to that of another Lorentz violation model—the QED-extension limit of standard model [46]. Also, it was found in [47] that both the first and the second kind of aether black holes have larger damping rates and smaller real oscillation frequencies of QNMs than Schwarzschild black holes.

The work is organized as follows. In Sect. 2 after giving a brief review of the BTZ black hole, we discuss the three-dimensional Hořava gravity and its connection with three-dimensional Einstein-aether theory. In Sect. 3 we find the QNMs analytically for massive scalar fields with circular symmetry and for a specify value of J. Also, for a massive scalar field we show that the Klein–Gordon equation can be written as the Heun equation, and we find the QNFs numerically by applying the pseudospectral method. Finally, our conclusions are in Sect. 4.

2 Three-dimensional rotating Hořava black holes

In this section, after reviewing in brief the BTZ black hole, we discuss the Hořava gravity and its connection with three-dimensional Einstein-aether theory. The metric of the BTZ black hole is given by

$$\begin{aligned} \mathrm{d}s^2 =& -\sinh^2\mu\,(r_+\mathrm{d}t - r_-\mathrm{d}\phi)^2 + \mathrm{d}\mu^2 \\ &+ \cosh^2\mu\,(-r_-\mathrm{d}t + r_+\mathrm{d}\phi)^2\,. \end{aligned} \tag{1}$$

The angular coordinate ϕ has period 2π, and the radii of the inner and outer horizons are denoted by r_- and r_+, respectively. The dual conformal field theory on the boundary is $(1+1)$-dimensional, the conformal symmetry being generated by two copies of the Virasoro algebra acting separately on left- and right-moving sectors [26]. Consequently, the conformal field theory splits into two independent sectors at thermal equilibrium with temperatures

$$T_{\mathrm{L}} = (r_+ - r_-)/2\pi\,, \quad T_{\mathrm{R}} = (r_+ + r_-)/2\pi. \tag{2}$$

According to the $\mathrm{AdS}_3/\mathrm{CFT}_2$ correspondence, to each field of spin s propagating in AdS_3 there corresponds an operator $\mathcal{O}$ in the dual conformal field theory characterized by conformal weights $(h_{\mathrm{L}}, h_{\mathrm{R}})$ with [25]

$$h_{\mathrm{R}} + h_{\mathrm{L}} = \Delta\,, \quad h_{\mathrm{R}} - h_{\mathrm{L}} = \pm s, \tag{3}$$

and Δ is determined in terms of the mass m of the scalar field,

$$\Delta = 1 + \sqrt{1+m^2}. \tag{4}$$

For a small perturbation, one expects that at late times the perturbed system will approach equilibrium exponentially with a characteristic time-scale. This time-scale is inversely proportional to the imaginary part of the poles, in momentum space, of the correlation function of the perturbation operator $\mathcal{O}$. For a conformal field theory at zero temperature, the 2-point correlation functions can be determined, up to normalization, from conformal invariance.

Then two sets of poles were found [26]:

$$\begin{aligned} \omega_{\mathrm{L}} &= k - 4\pi i T_{\mathrm{L}}(n + h_{\mathrm{L}}), \\ \omega_{\mathrm{R}} &= -k - 4\pi i T_{\mathrm{R}}(n + h_{\mathrm{R}}), \end{aligned} \tag{5}$$

where n takes the integer values $(n = 0, 1, 2, \ldots)$. This set of poles characterizes the decay of the perturbation on the CFT side, and coincides precisely with the quasinormal frequencies of the BTZ black hole [26].

We now discuss the three-dimensional Hořava gravity, the action of which is given by [48]

$$S_{\mathrm{H}} = \frac{1}{16\pi G_{\mathrm{H}}} \int \mathrm{d}T\,\mathrm{d}^2x N\sqrt{g}\,[L_2 + L_4]\,, \tag{6}$$

where G_{H} is a coupling constant with dimensions of a length squared and the Lagrangian L_2 has the following form:

$$L_2 = K_{ij}K^{ij} - \lambda K^2 + \xi\left({}^{(2)}R - 2\Lambda\right) + \eta a_i a^i, \tag{7}$$

where K_{ij}, K, and ${}^{(2)}R$ correspond to extrinsic, mean, and scalar curvature, respectively, and a_i is a parameter related to the lapse function N via $a_i = \partial_i \ln N$, being the line element in the preferred foliation

$$\mathrm{d}s^2 = N^2\mathrm{d}T^2 - g_{ij}(\mathrm{d}x^i + N^i\mathrm{d}T)(\mathrm{d}x^j + N^j\mathrm{d}T). \tag{8}$$

Also, g is the determinant of the induced metric g_{ij} on the constant-T hypersurfaces. L_4 corresponds to a set of all the terms with four spatial derivatives that are invariant under diffeomorphisms. For $\lambda = \xi = 1$ and $\eta = 0$, the action reduces to that of General Relativity. In the infrared limit of the theory the higher order terms L_4 (UV regime) can be neglected, and the theory is equivalent to a restricted version of Einstein-aether theory, through

$$u_\alpha = \frac{\partial_\alpha T}{\sqrt{g^{\mu\nu}\partial_\mu T\,\partial\nu T}} \tag{9}$$

and

$$\frac{G_H}{G_{\rm ae}} = \xi = \frac{1}{1-c_{13}}\,,\ \frac{\lambda}{\xi} = 1 + c_2\,,\ \frac{\eta}{\xi} = c_{14}\,, \tag{10}$$

where $c_{ij} = c_i + c_j$. With the action of the Einstein-aether:

$$S_{\rm ae} = \frac{1}{16\pi G_{\rm ae}}\int {\rm d}^3x\sqrt{-g}\,(-R - 2\Lambda + L_{\rm ae})\,, \tag{11}$$

where $G_{\rm ae}$ is a coupling constant with dimensions of a length square, g is the determinant of $g_{\mu\nu}$, Λ is the cosmological constant, R is the $3D$ Ricci scalar,

$$L_{\rm ae} = -M^{\alpha\beta\mu\nu}\nabla_\alpha u_\mu \nabla_\beta u_\nu, \tag{12}$$

and

$$M^{\alpha\beta\mu\nu} = c_1 g^{\alpha\beta}g^{\mu\nu} + c_2 g^{\alpha\mu}g^{\beta\nu} + c_3 g^{\alpha\nu}g^{\beta\mu} + c_4 u^\alpha u^\beta g^{\mu\nu}. \tag{13}$$

Another important characteristic of this theory is that only in the sector $\eta = 0$, Hořava gravity admits an asymptotically AdS solution [29]. Therefore, assuming stationary and circular symmetry, the theory will admit the BTZ analogue to the three-dimensional rotating Hořava black holes described by the metric

$${\rm d}s^2 = Z(r)^2{\rm d}t^2 - \frac{1}{F(r)^2}{\rm d}r^2 - r^2({\rm d}\phi + \Omega(r){\rm d}t)^2, \tag{14}$$

where

$$F(r)^2 = Z(r)^2 = -M + \frac{\bar{J}^2}{4r^2} - \bar{\Lambda}r^2, \tag{15}$$

with

$$\bar{J}^2 = \frac{J^2 + 4a^2(1-\xi)}{\xi},\ \Omega(r) = -\frac{J}{2r^2},\ \bar{\Lambda} = \Lambda - \frac{b^2(2\lambda - \xi - 1)}{\xi}, \tag{16}$$

where a and b are constants that can be regarded as measures of aether misalignment, with b a measure of asymptotically misalignment, for $b \neq 0$, the aether does not align with the timelike Killing vector asymptotically. Note that when $\xi = 1$ and $\lambda = 1$, the solution becomes that of BTZ black holes, and for $\xi = 1$, the solution becomes "BTZ black holes" with a shifted cosmological constant, $\bar{\Lambda} = \Lambda - 2b^2(\lambda - 1)$. However, there is still a preferred direction represented by the aether vector field which breaks Lorentz invariance for $\lambda \neq 1$ and $b \neq 0$. Also, $\bar{J}^2$ can be negative, when either $\xi < 0$ or $\xi > 1$, $a^2 > J^2/(4(\xi - 1))$. The sign of $\bar{\Lambda}$ determines the asymptotic behavior (flat, dS, or AdS) of the metric [29]; here we focus on the AdS sector.

In [29] it was argued that, if $\xi > 0$ and $\lambda > 0$, the aether represents a well-defined folation at large r for any value of b. Moreover, if $\lambda \geq (1+\xi)/2$, then $\bar{\Lambda}$ is always negative for any b. Also, if the coupling constants are such that $\xi > 0$, $\lambda > 1/2$ and $\lambda < (1+\xi)/2$, then $\bar{\Lambda}$ will switch sign at some value of b.

In Fig. 1 we show the behavior of $F(r)^2$ as a function of r. When ξ increases (left panel), we observe a region where there is no a horizon until $\xi = \xi_{\mathbf{e}}$ for which the black hole becomes extremal; this value can be obtained from $r_- = r_+$. Then there is a region where r_+ increases and r_- decreases until it becomes null when $\xi = \xi_c$, and finally there is a region $\xi > \xi_c$ where there is only one horizon. Also, we can observe the same behavior when λ decreases (right panel). In Figs. 2 and 3, we plot the behavior of $\bar{\Lambda}$ as a function of b, and its sign determines the asymptotic behavior (flat, dS, or AdS) of the metric. Note that, for $-1.4 < b < 1.4$, the sign of $\bar{\Lambda}$ is negative, as mentioned, if the coupling constants are such that $\xi > 0$, $\lambda > 1/2$ and $\lambda < (1+\xi)/2$, then $\bar{\Lambda}$ will switch sign at some value of b.

The value of ξ for which the black hole is extremal is given by

$$\xi_{\rm e} = -\frac{1}{2(M^2 - 4a^2(b^2+\Lambda))}\Big(b^2(J^2 + 8a^2\lambda) + \Lambda(J^2 + 4a^2) - \Big((b^2(J^2 + 8a^2\lambda) + \Lambda(J^2 + 4a^2))^2 + 4b^2(J^2 + 4a^2)(2\lambda - 1)(M^2 - 4a^2(b^2 + \Lambda))\Big)^{1/2}\Big), \tag{17}$$

the value of ξ for which the black hole passes from having two horizons to having one horizon is given by

$$\xi_{\rm c} = \frac{4a^2 + J^2}{4a^2}, \tag{18}$$

and the value of ξ for which the effective cosmological constant $\bar{\Lambda}$ changes sign is given by $\xi = \frac{(2\lambda-1)b^2}{b^2+\lambda}$. In Fig. 4, we plot the different regions defined by $\xi_{\rm e}$, $\xi_{\rm c}$, and $\bar{\Lambda}$ for a choice of parameters.

In the case $\bar{J} \neq J$ ($\xi \neq 1$), there is a curvature singularity due to the Ricci scalar

$$R = -6\bar{\Lambda} + \frac{1}{2r^2}\left(\bar{J}^2 - J^2\right) \tag{19}$$

being divergent at $r = 0$. This is in contrast to BTZ black holes where the Ricci and Kretschmann scalars are finite and smooth at $r = 0$. The locations of the inner and outer

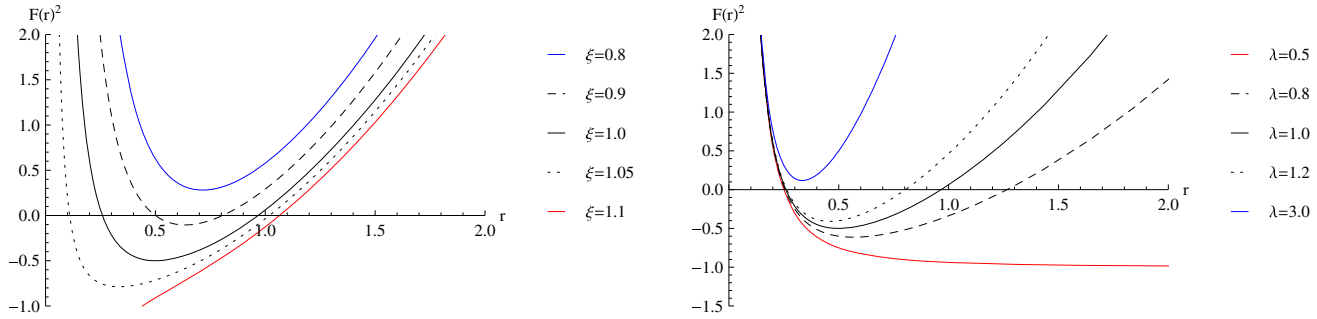

Fig. 1 The behavior of $F(r)^2$ as a function of r, with $M = 1$, $a = 1$, $b = 1$, $\Lambda = -1$, $J = 0.5$. Left panel for $\lambda = 1$ and right panel for $\xi = 1$

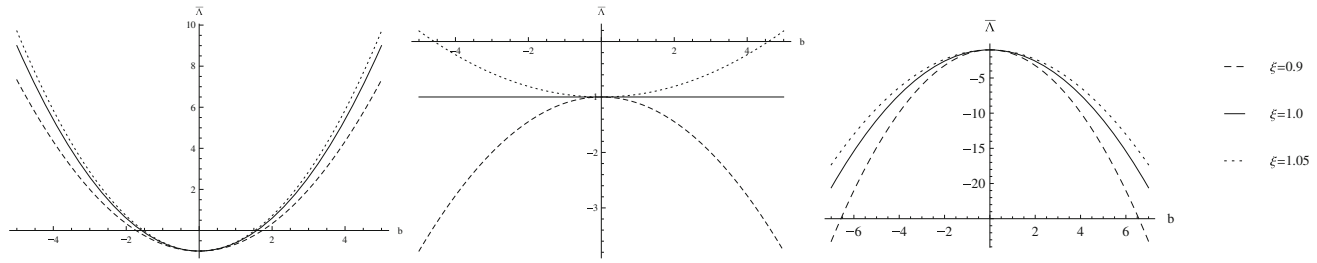

Fig. 2 The behavior of $\bar{\Lambda}$ as a function of b, with $\Lambda = -1$. Left panel for $\lambda = 0.8$, central panel for $\lambda = 1$ and right panel for $\lambda = 1.2$

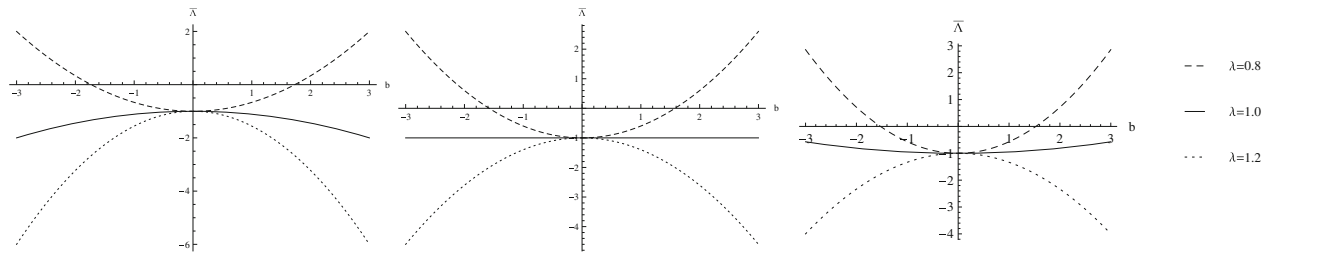

Fig. 3 The behavior of $\bar{\Lambda}$ as a function of b, with $\Lambda = -1$. Left panel for $\xi = 0.9$, central panel for $\xi = 1$ and right panel for $\xi = 1.05$

horizons, $r = r_{\pm}$, are given by

$$r_{\pm}^2 = -\frac{M}{2\bar{\Lambda}}\left(1 \pm \sqrt{1 + \frac{\bar{J}^2\bar{\Lambda}}{M^2}}\right). \tag{20}$$

Also, M and $\bar{J}$ can be written as $M = -\bar{\Lambda}(r_+^2 + r_-^2)$ and $\bar{J} = 2r_+r_-\sqrt{-\bar{\Lambda}}$, respectively. The Hawking temperature T_H is given by

$$T_H = \frac{-\bar{\Lambda}(r_+^2 - r_-^2)}{2\pi r_+}. \tag{21}$$

3 QNMs

The quasinormal modes of scalar perturbations for a minimally coupled massive scalar field to curvature on the background of three-dimensional Hořava AdS black holes are described by the solution of the Klein–Gordon equation

$$\Box\psi = \frac{1}{\sqrt{-g}}\partial_\mu\left(\sqrt{-g}g^{\mu\nu}\partial_\nu\right)\psi = -m^2\psi, \tag{22}$$

where m is the mass of the scalar field ψ. As was argued in Ref. [49], it is possible to consider the usual Klein–Gordon equation by neglecting the possible strong coupling of the scalar mode in the Hořava gravity [50,51] due to the scalar field considered being just a probe field that perturbs the background and does not have the symmetries of the background metric and one understands the symmetries only through the background metric, which is the standard procedure to compute the QNMs. Only if the scalar field backreacts to the metric it can correspond to the symmetries of the background metric but this matter is not considered in our study. Also, at large distances and relatively small momenta the corrections to the ordinary Lorentz-invariant physics should be relatively small. Equation (22) can be written as

$$\left(-\frac{1}{F(r)^2}\partial_t^2 + F(r)^2\partial_r^2 + \frac{1}{r}\partial_r(rF(r)^2)\partial_r - \frac{J}{r^2F(r)^2}\partial_t\partial_\phi\right.$$

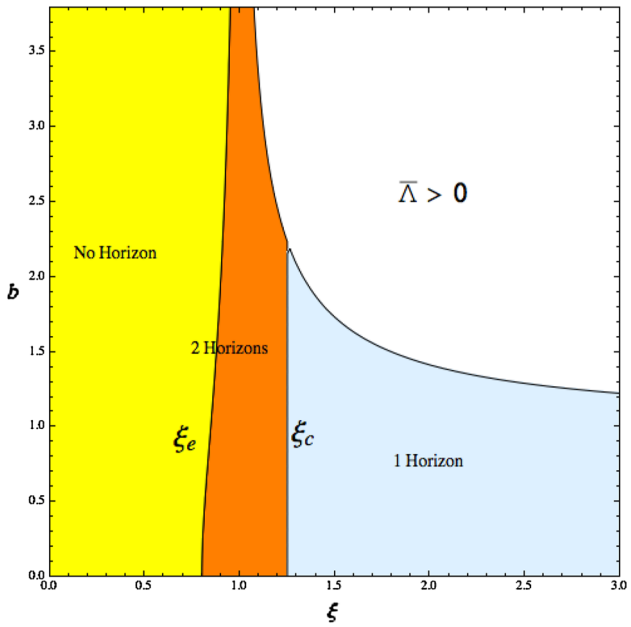

Fig. 4 Different regions of the parameter space for $a = 1$, $\lambda = 1$, $\Lambda = -1$, $M = 1.5$ and $J = 1$. The colored region corresponds to $\bar{\Lambda} < 0$. In the yellow regions, there are no black hole solutions. In the orange region, the black holes have two horizons while in the light blue region, they have one horizon

$$+\frac{1}{r^2F(r)^2}(F(r)^2-\frac{J^2}{4r^2})\partial_\phi^2-m^2\Big)\psi=0. \tag{23}$$

The term $F(r)^2-\frac{J^2}{4r^2}$ is given by

$$\begin{aligned}
&-M+\frac{\bar{J}^2}{4r^2}-\bar{\Lambda}r^2-\frac{J^2}{4r^2}\\
&=-M+\frac{J^2+4a^2(1-\xi)}{4\xi r^2}\\
&\quad-(\Lambda-\frac{b^2(2\lambda-\xi-1)}{\xi})r^2-\frac{J^2}{4r^2}\\
&=-M+\frac{J^2}{4r^2}\left(\frac{1}{\xi}+\frac{4a^2(1-\xi)}{\xi}-1\right)\\
&\quad-\left(\Lambda-\frac{b^2(2\lambda-\xi-1)}{\xi}\right)r^2.
\end{aligned} \tag{24}$$

It is worth mentioning that the second term in the above expression vanishes for $\xi = 1$. Performing the change of variables $z=\frac{r^2-r_+^2}{r^2-r_-^2}$ along with the ansatz $\psi = R(z)e^{-i\omega t}e^{i\kappa\phi}$, Eq. (23) yields

$$\begin{aligned}
&z(1-z)\partial_z^2R(z)+(1-z)\,\partial_zR(z)\\
&+\Bigg[-\frac{\omega^2(zr_-^2-r_+^2)}{4\bar{\Lambda}^2(r_+^2-r_-^2)^2z}-\frac{J\omega\kappa}{4\bar{\Lambda}^2(r_+^2-r_-^2)^2}\frac{1-z}{z}\\
&-\frac{\kappa^2}{4\bar{\Lambda}^2(r_+^2-r_-^2)^2}\left(F(z)^2-\frac{J^2}{4r(z)^2}\right)\frac{1-z}{z}\\
&+\frac{m^2}{4(1-z)\bar{\Lambda}}\Bigg]R(z)=0.
\end{aligned} \tag{25}$$

3.1 Massive scalar field with circular symmetry

For a massive scalar field with circular symmetry ($\kappa = 0$) Eq. (25) is

$$\begin{aligned}
&z(1-z)\partial_z^2R(z)+(1-z)\,\partial_zR(z)\\
&+\left[-\frac{\omega^2(zr_-^2-r_+^2)}{4\bar{\Lambda}^2(r_+^2-r_-^2)^2z}+\frac{m^2}{4(1-z)\bar{\Lambda}}\right]R(z)=0,
\end{aligned} \tag{26}$$

which can be written as

$$\begin{aligned}
&z(1-z)\partial_z^2R(z)+(1-z)\,\partial_zR(z)\\
&+\left(A+\frac{B}{z}+\frac{C}{1-z}\right)R(z)=0,
\end{aligned} \tag{27}$$

where

$$A=-\frac{\omega^2r_-^2}{4\bar{\Lambda}^2(r_+^2-r_-^2)^2},\ B=\frac{\omega^2r_+^2}{4\bar{\Lambda}^2(r_+^2-r_-^2)^2},\ C=\frac{m^2}{4\bar{\Lambda}}. \tag{28}$$

Under the decomposition $R(z)=z^\alpha(1-z)^\beta K(z)$, Eq. (27) can be written as a hypergeometric equation for K

$$z(1-z)K''(z)+[c_1-(1+a_1+b_1)z]\,K'(z)-a_1b_1K(z)=0, \tag{29}$$

where the coefficients a_1, b_1, and c_1 are given by

$$a_1=\alpha+\beta\mp\sqrt{A},\ b_1=\alpha+\beta\pm\sqrt{A}\ ,\ c_1=1+2\alpha, \tag{30}$$

and the exponents α and β are

$$\alpha=\pm i\sqrt{B},\ \beta=\frac{1}{2}\left(1\pm\sqrt{1-4C}\right). \tag{31}$$

The general solution of Eq. (29) takes the form

$$\begin{aligned}
K&=C_1\,{}_2F_1(a_1,b_1,c_1;z)\\
&\quad+C_2z^{1-c}\,{}_2F_1(a_1-c_1+1,b_1-c_1+1,2-c_1;z),
\end{aligned} \tag{32}$$

which has three regular singular points at $z = 0$, $z = 1$, and $z = \infty$. Here, ${}_2F_1(a_1, b_1, c_1; z)$ is a hypergeometric function and C_1, C_2 are constants. Then, without loss of generality, we choose the negative sign for α, and the solution for the radial function $R(z)$ is

$$\begin{aligned}
R(z)&=C_1z^\alpha(1-z)^\beta\,{}_2F_1(a_1,b_1,c_1;z)\\
&\quad+C_2z^{-\alpha}(1-z)^\beta\,{}_2F_1(a_1-c_1\\
&\quad+1,b_1-c_1+1,2-c_1;z).
\end{aligned} \tag{33}$$

According to our change of variables at the vicinity of the horizon $r\to r_+$, $z\to 0$, and at infinity $r\to\infty$, $z\to 1$.

In the vicinity of the horizon, $z = 0$ and using the property $F(a_1, b_1, c_1, 0) = 1$, the function $R(z)$ behaves as

$$R(z) = C_1 e^{\alpha \ln z} + C_2 e^{-\alpha \ln z}, \tag{34}$$

and the scalar field ψ can be written in the following way:

$$\psi \sim C_1 e^{-i\omega(t+\frac{r_+}{2|\bar{\Lambda}|(r_+^2-r_-^2)}\ln z)} + C_2 e^{-i\omega(t-\frac{r_+}{2|\bar{\Lambda}|(r_+^2-r_-^2)}\ln z)} \tag{35}$$

in which the first term represents an ingoing wave and the second term an outgoing wave in the black hole. To compute the QNMs, we have to impose the boundary conditions on the horizon that there exist only ingoing waves. This fixes $C_2 = 0$. So, the radial solution becomes

$$\begin{aligned} R(z) &= C_1 e^{\alpha \ln z}(1-z)^{\beta} F_1(a_1, b_1, c_1; z) \\ &= C_1 e^{-i\omega\frac{r_+}{2|\bar{\Lambda}|(r_+^2-r_-^2)}\ln z}(1-z)^{\beta} F_1(a_1, b_1, c_1; z)\ . \end{aligned} \tag{36}$$

In order to implement boundary conditions at infinity ($z = 1$), we shall apply in Eq. (36) Kummer's formula, for the hypergeometric function [52],

$$\begin{aligned} &{}_2F_1(a_1, b_1, c_1; z) \\ &= \frac{\Gamma(c_1)\Gamma(c_1 - a_1 - b_1)}{\Gamma(c_1 - a_1)\Gamma(c_1 - b_1)}\, {}_2F_1(a_1, b_1, a_1 + b_1 - c_1, 1 - z) \\ &\quad + (1-z)^{c_1 - a_1 - b_1}\frac{\Gamma(c)\Gamma(a_1 + b_1 - c_1)}{\Gamma(a_1)\Gamma(b_1)}\, {}_2F_1(c_1 \\ &\quad - a_1, c_1 - b_1, c_1 - a_1 - b_1 + 1, 1 - z). \end{aligned} \tag{37}$$

With this expression, the radial function results in

$$\begin{aligned} R(z) &= C_1 e^{-i\omega\frac{r_+}{2|\bar{\Lambda}|(r_+^2-r_-^2)}\ln z} \\ &\quad (1-z)^{\beta}\frac{\Gamma(c_1)\Gamma(c_1 - a_1 - b_1)}{\Gamma(c_1 - a_1)\Gamma(c_1 - b_1)}\, {}_2F_1(a_1, b_1, a_1 \\ &\quad + b_1 - c_1, 1 - z) + C_1 e^{-i\omega\frac{r_+}{2|\bar{\Lambda}|(r_+^2-r_-^2)}\ln z} \\ &\quad (1-z)^{c_1 - a_1 - b_1 + \beta}\frac{\Gamma(c_1)\Gamma(a_1 + b_1 - c_1)}{\Gamma(a_1)\Gamma(b_1)}\, {}_2F_1(c_1 \\ &\quad - a_1, c_1 - b_1, c_1 - a_1 - b_1 + 1, 1 - z). \end{aligned} \tag{38}$$

Therefore, by imposing the requirement that the scalar field at infinity is null, for $m^2/\bar{\Lambda} < 0$ ($\beta_- < 0$ and $c_1 - a_1 - b_1 + \beta_- = \beta_+ > 0$), the term proportional to $(1-z)^{\beta}$ in Eq. (38) diverges. So, we find that the scalar field is null only upon setting the additional restriction $(c_1 - a_1)|_{\beta_-} = -n$ or $(c_1 - b_1)|_{\beta_-} = -n$. Then the QNFs yields

$$\omega_1 = -i|\bar{\Lambda}|\left(\sqrt{1-4C} + 2n + 1\right)(r_- + r_+), \tag{39}$$

$$\omega_2 = -i|\bar{\Lambda}|\left(\sqrt{1-4C} + 2n + 1\right)(r_+ - r_-), \tag{40}$$

respectively. Note that the imaginary part of the QNFs is negative, which ensures that the propagation of scalar fields is stable in this background.

Now, in order to observe the behavior of the QNFs (39) and (40), we plot in Fig. 5, the behavior of the real (left panel) and imaginary parts (right panel) of the fundamental QNFs as a function of ξ. Note that, as mentioned, for $\xi < \xi_e$, there is no horizon. So, for $\xi > \xi_e$, we observe that for ω_1 (continuous line) there is a range where $Re(\omega_1)$ is null and then takes positive values, when the coupling constant ξ increases, while $|\mathrm{Im}(\omega_1)|$ decreases when ξ increases. So, according to the gauge/gravity duality, the relaxation time in order to reach the thermal equilibrium increases for the right sector. However, for ω_2 (dashed line) and $\xi > \xi_e$, $\mathrm{Re}(\omega_2)$ is null and then takes negative values, while its imaginary part increases and then decreases when the coupling constant ξ increases, showing that the relaxation time can decrease or increase depending on the value of ξ. It is interesting to note that when $\mathrm{Im}(\omega_2)$ decreases $\mathrm{Im}(\omega_1) = \mathrm{Im}(\omega_2)$. If we consider the BTZ black hole, $\xi = 1$ and $\lambda = 1$, the real part is null and $\mathrm{Im}(\omega_1) \neq \mathrm{Im}(\omega_2)$. In the following, we will analyze the two branches of QNFs for different values of ξ. Figure 6 is similar to Fig. 5, but in order to see the effect of b on the behavior of the QNFs, we have plotted several curves corresponding to different values of parameter b. For $\xi = 1$ the QNFs coincide and correspond to the QNFs of the BTZ black hole. On the other hand, for $\xi = \xi_c$, the two purely imaginary branches converge to the same value. For values of ξ near 1, $|\mathrm{Im}(\omega_1)|$ decreases when ξ increases, decreasing faster for large values of b, while $|\mathrm{Im}(\omega_2)|$ increases when ξ increases, increasing faster for small values of b, which implies that the relaxation time of the right sector increases and the relaxation time of the left sector decreases. On the other hand, we observe that, for ξ near ξ_c with $\xi > \xi_c$, only one branch exists, and $|\mathrm{Im}(\omega)|$ decreases for small values of b, while it increases for large values of b. Notice that for $b = 3$ the effective cosmological constant $\bar{\Lambda}$ becomes positive before reaching the value ξ_c.

3.1.1 $\xi_e < \xi < \xi_c$

Now, in order to observe the behavior of the QNFs (39) and (40), in the range $\xi_e < \xi < \xi_c$, that is, where $r_\pm$ are positive, first we plot $r_\pm$ versus J in Fig. 7, for different values of the parameters ξ and λ, in order to see for which values of the parameter J the horizons $r_\pm$ are positive. Then, for this range, we plot the imaginary part $\mathrm{Im}(\omega)$ of the QNFs in Fig. 8, and we observe that, for ω_1, $|\mathrm{Im}(\omega_1)|$ increases when the parameter J (or equivalently $\bar{J}$; see Fig. 9) increases; see left panel of Fig. 8, so the relaxation time decreases. However, for ω_2, the behavior is the opposite. $|\mathrm{Im}(\omega_2)|$ decreases when the parameter J increases; see the right panel of Fig. 8, so the relaxation time increases. Note that in this range $\mathrm{Re}(\omega)$ is null. Also, the sectors T_R and T_L of the conformal field theory are well defined. Furthermore, $|\mathrm{Im}(\omega_1)|$ decreases and $|\mathrm{Im}(\omega_2)|$ increases, when the coupling constant ξ increases; so, the relaxation time increases and decreases, respectively.

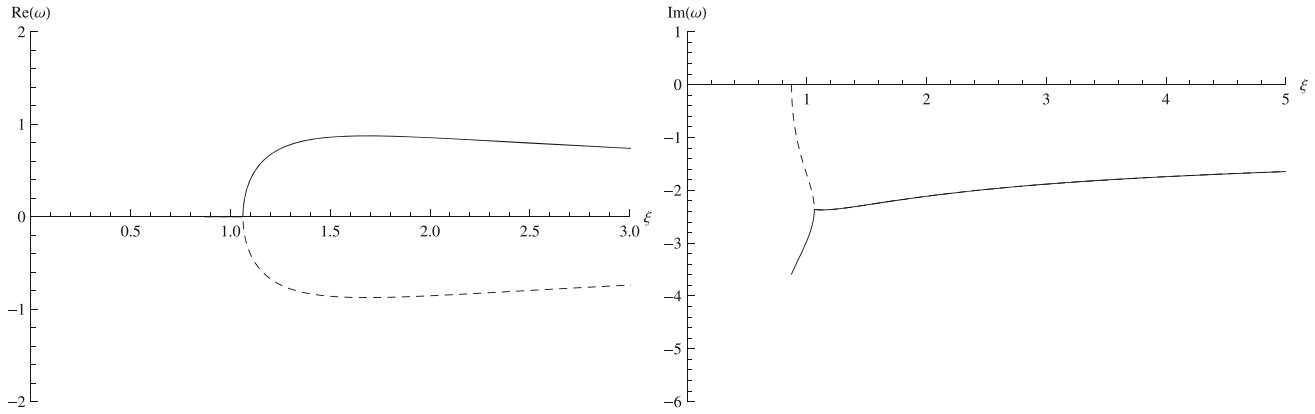

Fig. 5 The fundamental QNFs for $M = 1$, $\lambda = 1$, $\Lambda = -1$, $a = b = m = 1$, and $J = 0.5$, as a function of ξ. Left panel for $Re(\omega)$, and right panel for $Im(\omega)$. Continuous line for ω_1, and dashed line for ω_2

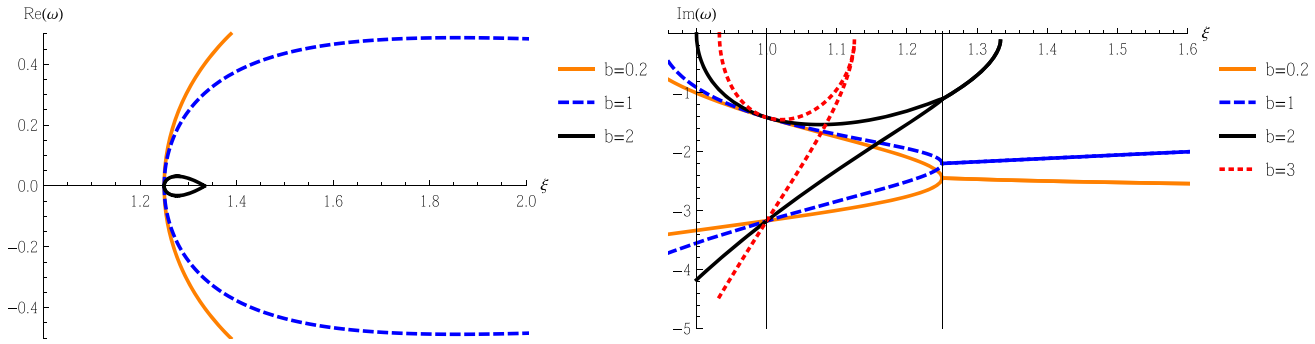

Fig. 6 The fundamental QNFs for $M = 1.5$, $\lambda = 1$, $\Lambda = -1$, $a = 1$, $m = 0.1$, $J = 1$ and $b = 0.2, 1, 2, 3$ as a function of ξ. Left panel for $Re(\omega)$, and right panel for $Im(\omega)$. In the right panel, the upper curves correspond to the ω_1 branch, while the lower curves correspond to the ω_2 branch. For $\xi = 1$ all the frequencies coincide with the frequencies of BTZ black holes. For $\xi_c = 1.25$, both branches converge. For $\xi < \xi_c$ the QNFs are purely imaginary, while that for $\xi > \xi_c$ acquire a real part. For $b = 3$, the frequencies are purely imaginary

In Fig. 10 we plot the fundamental QNFs as a function of b. We observe that, for the BTZ black hole, the central panel with $\xi = 1$, the imaginary part of the fundamental QNF is constant; however, for an asymptotical misalignment of the aether with the timelike Killing vector, $b \neq 0$, the fundamental QNFs depend on b. $|\mathrm{Im}(\omega_1)|$ increases when ξ decreases. For $|\mathrm{Im}(\omega_2)|$ the behavior is the opposite since it decreases when ξ decreases.

3.1.2 $\xi > \xi_c$

As mentioned, for $\xi > \xi_c$ there is only one horizon. $r_+ > 0$ and r_- become imaginary. This occurs for $\xi > (J^2 + 4a^2)/(4a^2)$, and consequently there is a gap in J; see Fig. 7, left panel, and for which $\bar{J}^2$ is negative; see Fig. 9, which occurs when $J^2 < 4a^2(\xi - 1)$. In Fig. 11, we plot the fundamental QNFs for the range of values of J in which it is positive, and there is only one horizon. So, we observe that the fundamental QNFs acquire a real part, with $\mathrm{Re}(\omega_1) = -\mathrm{Re}(\omega_2)$, $|\mathrm{Re}(\omega)|$ decreasing when J increases, and $\mathrm{Im}(\omega_1) = \mathrm{Im}(\omega_2)$, and it is negative. In this case, the two branches show convergence to one branch and when the coupling constant ξ increases $|\mathrm{Im}(\omega)|$ decreases; see Fig. 5.

3.1.3 $\xi = \xi_c$

Finally, for $\xi = \xi_c$, that is, $r_- = 0$, the two sectors converge, this occurs for $\bar{J} = 0$, that is, $J^2 + 4a^2(1 - \xi) = 0$. In this case the QNFs are given by

$$\omega_1 = \omega_2 = -i|\bar{\Lambda}|r_+\left(\sqrt{1 - 4C} + 2n + 1\right), \tag{41}$$

where $r_+^2 = -\frac{M}{\bar{\Lambda}}$. In Fig. 12 we show the behavior of the fundamental QNFs as a function of $\xi = \xi_c$. We observe that $|\mathrm{Im}(\omega)|$ decreases when ξ_c increases whereas $\mathrm{Re}(\omega)$ is null. So, according to the gauge/gravity duality, the relaxation time in order to reach the thermal equilibrium increases.

Finally, we plot in Fig. 13 $\mathrm{Im}(\omega)$ for different values of the constants a and b. We observe that, for the range $\xi > \xi_e$, $|\mathrm{Im}(\omega)|$ increases when the constants a or b increase, so the relaxation time decreases.

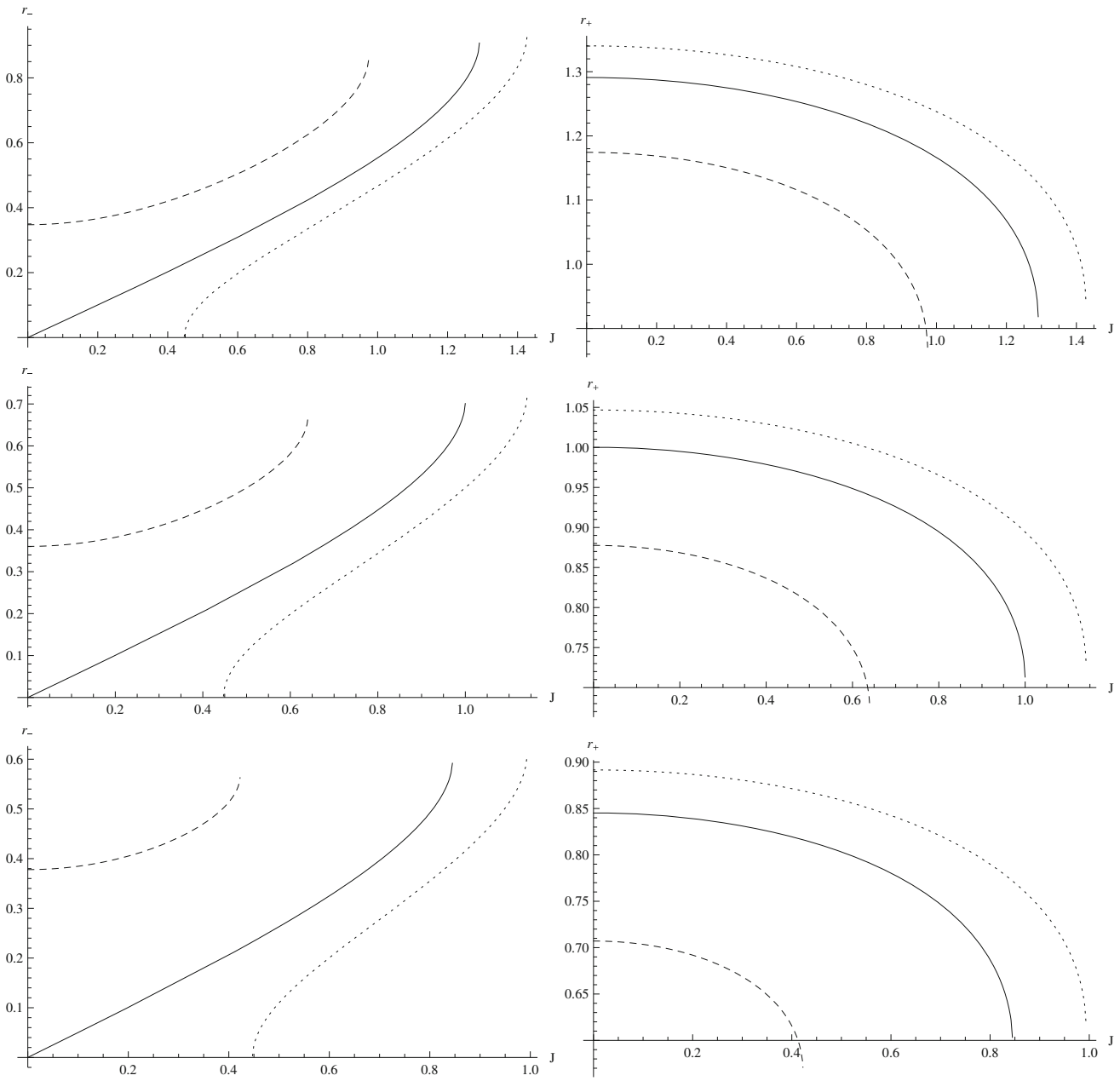

Fig. 7 The behavior of r_- (left) and r_+ (right) as a function of J, with $M = 1$, $a = 1$, $b = 1$, and $\Lambda = -1$, dashed lines for $\xi = 0.9$, continuous lines for $\xi = 1.0$, and dotted lines for $\xi = 1.05$. Top panels for $\lambda = 0.8$, central panels for $\lambda = 1.0$, and bottom panels for $\lambda = 1.2$

Neumann boundary conditions The frequencies found above for the scalar perturbation have been obtained by imposing the vanishing Dirichlet boundary condition at infinity. It is well known that the Dirichlet boundary condition does not lead to any QNMs for $m^2 < 0$. However, it is also possible to find a second set of QNFs, for negative mass squared, if we consider that the flux of the scalar field vanishes at infinity or vanishing Neumann boundary condition at infinity, which allows us to describe tachyons. Furthermore, it was shown that for negative mass squared there are two sets of dual operators Δ_+ and Δ_-, where the second set of QNFs matches exactly the dual operators with Δ_- [26]. So, by using the condition that the flux, which is given by

$$F = \frac{\sqrt{-g}g^{rr}}{2i}(\psi^*\partial_r\psi - \psi\partial_r\psi^*), \tag{42}$$

vanishes at asymptotic infinity, we find, for $\beta = \beta_-$ and $0 > m^2 > \bar{\Lambda}$, that the flux vanishes if $(a)|_{\beta_-} = -n$ or $(b)|_{\beta_+} = -n$, which leads to

$$\omega = -i|\bar{\Lambda}|\left(-\sqrt{1-4C}+2n+1\right)(r_+ - r_-), \tag{43}$$

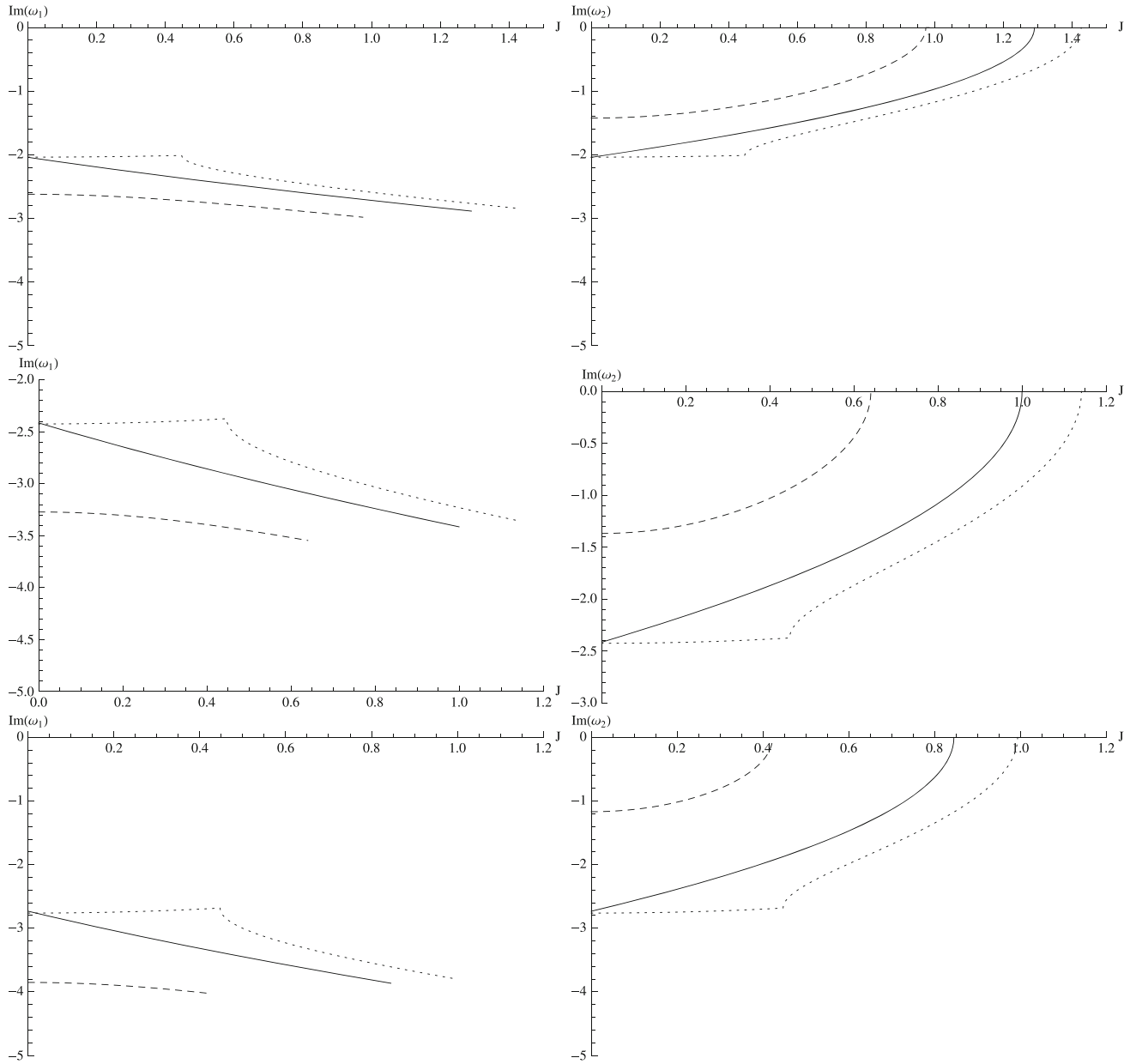

Fig. 8 The fundamental QNFs ω_1 (left) and ω_2 (right) as a function of J with $M = 1$, $a = 1$, $b = 1$, $\Lambda = -1$, $m = 1$. Top panels for $\lambda = 0.8$, central panels for $\lambda = 1$ and bottom panels for $\lambda = 1.2$. Dashed lines for $\xi = 0.9$, continuous lines for $\xi = 1.0$ and dotted lines for $\xi = 1.05$

$$\omega = -i\,|\bar{\Lambda}|\left(-\sqrt{1-4C}+2n+1\right)(r_- + r_+), \tag{44}$$

respectively.

3.2 Massive scalar field

For massive scalar field, the Klein–Gordon equation can be rewritten as

$$z(1-z)\partial_z^2 R(v) + (1-z)\,\partial_z R(z) + \left[A + \frac{B}{z} + \frac{C}{1-z} + \frac{D}{\bar{a}-z}\right] R(z) = 0, \tag{45}$$

where

$$A = -\frac{(\omega r_- - \kappa r_+)^2}{4\bar{\Lambda}^2(r_+^2 - r_-^2)^2},\ B = \frac{(\omega r_+ - \kappa r_-)^2}{4\bar{\Lambda}^2(r_+^2 - r_-^2)^2},\ C = \frac{m^2}{4\bar{\Lambda}},$$
$$D = \frac{\kappa^2\left((-1+\bar{a})^2 J^2 + 4\bar{a}\bar{\Lambda}(r_-^2 - r_+^2)^2\right)}{16\bar{a}\bar{\Lambda}^2 r_-^2 (r_-^2 - r_+^2)^2}, \tag{46}$$

and

$$\bar{a} = r_+^2/r_-^2. \tag{47}$$

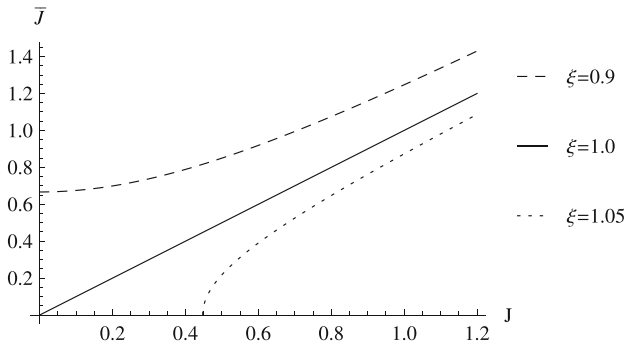

Fig. 9 The behavior of $\bar{J}$ as a function of J, with $a = 1$. Dashed line for $\xi = 0.9$, continuous line for $\xi = 1.0$ and dotted line for $\xi = 1.05$

Under the decomposition $R(z) = z^{\alpha}(1-z)^{\beta}(\bar{a}-z)K(z)$, with

$$\alpha = \pm i\sqrt{B},\ \beta = \frac{1}{2}\left(1 \pm \sqrt{1-4C}\right), \tag{48}$$

Eq. (45) can be written as

$$\partial_z^2 K(z) + \left(\frac{1+2\alpha}{z} - \frac{2\beta}{1-z} - \frac{2}{\bar{a}-z}\right)\partial_z R(z) + \frac{1}{(z)(1-z)(\bar{a}-z)}\left(q + \epsilon_1\epsilon_2 z\right)R(z) = 0, \tag{49}$$

where

$$q = -1 - B + C + D - 2\alpha - \alpha^2 - \beta + \beta^2 + \bar{a}\left(A - (\alpha+\beta)^2\right), \tag{50}$$

$$\epsilon_1 = -\sqrt{A} + (1+\alpha+\beta),\ \epsilon_2 = \sqrt{A} + (1+\alpha+\beta), \tag{51}$$

which corresponds to Heun's differential equation. The condition $2 = \epsilon_1 + \epsilon_2 - (1+2\alpha) - 2\beta + 1$, ensures regularity of the point at ∞, and q corresponds to the accessory parameter. Heun's equation has four regular singular points: 0, 1, a, and ∞ with exponents $(0, -2\alpha)$, $(0, 1-2\beta)$, $(0, -1)$, and (ϵ_1, ϵ_2). Now, in order to obtain the QNFs, we proceed to perform a numerical analysis by using the pseudospectral Chebyshev method [53], which has been applied to computing the QNFs in other geometries; for instance see [54–56]. In Fig. 14 we plot the numerical results obtained for the real and imaginary parts of the lowest QNF as a function of ξ for different values of κ. We observe that, for $\xi > 1$, the absolute value of the imaginary part decreases as κ increases; however, for $\xi < 1$, the behavior is the opposite; the absolute value of the imaginary part increases as κ increases. Note that, for the cases analyzed, the QNFs have a negative imaginary part, which ensures that the propagation of scalar fields is stable in this background.

3.3 Case: $J = \bar{J}$

In this case, Eq. (45) becomes

$$z(1-z)\partial_z^2 R(v) + (1-z)\,\partial_z R(z) + \left[A + \frac{B}{z} + \frac{C}{1-z}\right]R(z) = 0, \tag{52}$$

where A, B, and C are given by Eq. (46). Under the decomposition $R(z) = z^{\alpha}(1-z)^{\beta}K(z)$, Eq. (52) can be written as a hypergeometric equation for K, Eq. (29), where the coefficients a_1, b_1 and c_1 are given by

$$a_1 = \alpha + \beta \mp \sqrt{A},\ b_1 = \alpha + \beta \pm \sqrt{A},\ c_1 = 1 + 2\alpha, \tag{53}$$

and the exponents α and β are

$$\alpha = \pm i\sqrt{B},\ \beta = \frac{1}{2}\left(1 \pm \sqrt{1-4C}\right). \tag{54}$$

Following the same procedure as detailed in the case of massive radial scalar field we obtain for $m^2/\bar{\Lambda} < 0$ ($\beta_- < 0$ and $\beta_+ > 0$) the result that the field at infinity is null if the gamma function $\Gamma(x)$ has the poles at $x = -n$ for $n = 0, 1, 2, \ldots$. Then the wave function satisfies the considered boundary condition only upon setting the additional restriction $(c_1 - a_1)|_{\beta_-} = -n$ or $(c_1 - b_1)|_{\beta_-} = -n$. These conditions determine the form of the QNFs as

$$\omega_1 = -i|\bar{\Lambda}|(r_- + r_-)(2n + 1 + \sqrt{1-4C}) - \kappa\sqrt{-\bar{\Lambda}}, \tag{55}$$

$$\omega_2 = -i|\bar{\Lambda}|(r_+ - r_-)(2n + 1 + \sqrt{1-4C}) + \kappa\sqrt{-\bar{\Lambda}}, \tag{56}$$

respectively.

Now, in a similar manner to the first case, that is, using the condition that the flux vanishes at asymptotic infinity, we obtain for $\beta = \beta_+$ and $0 > m^2 > \bar{\Lambda}$, with $(b_1)|_{\beta_+} = -n$ or $(a_1)|_{\beta_-} = -n$, the second set of QNFs, which yields

$$\omega = -i|\bar{\Lambda}|(r_- + r_-)(2n + 1 - \sqrt{1-4C}) - \kappa\sqrt{-\bar{\Lambda}}, \tag{57}$$

$$\omega = -i|\bar{\Lambda}|(r_+ - r_-)(2n + 1 - \sqrt{1-4C}) + \kappa\sqrt{-\bar{\Lambda}}, \tag{58}$$

respectively. In this case, the QNFs correspond to $\omega = \omega_{\rm mr} \mp \kappa\sqrt{-\bar{\Lambda}}$, where $\omega_{\rm mr}$ are the QNFs for massive radial scalar fields. So, the condition $J = \bar{J}$, only has an effect on the real part of the QNFs. As mentioned, when $\xi = 1$ (J=$\bar{J}$), the solution results in the "BTZ black holes" with a shifted cosmological constant, $\bar{\Lambda} = \Lambda - 2b^2(\lambda - 1)$. However, there is still a preferred direction represented by the aether vector field which breaks Lorentz invariance for $\lambda \neq 1$ and $b \neq 0$. Note that the QNFs have real and imaginary parts, with an imaginary part that is negative, which ensures that the propagation of scalar fields is stable in this background.

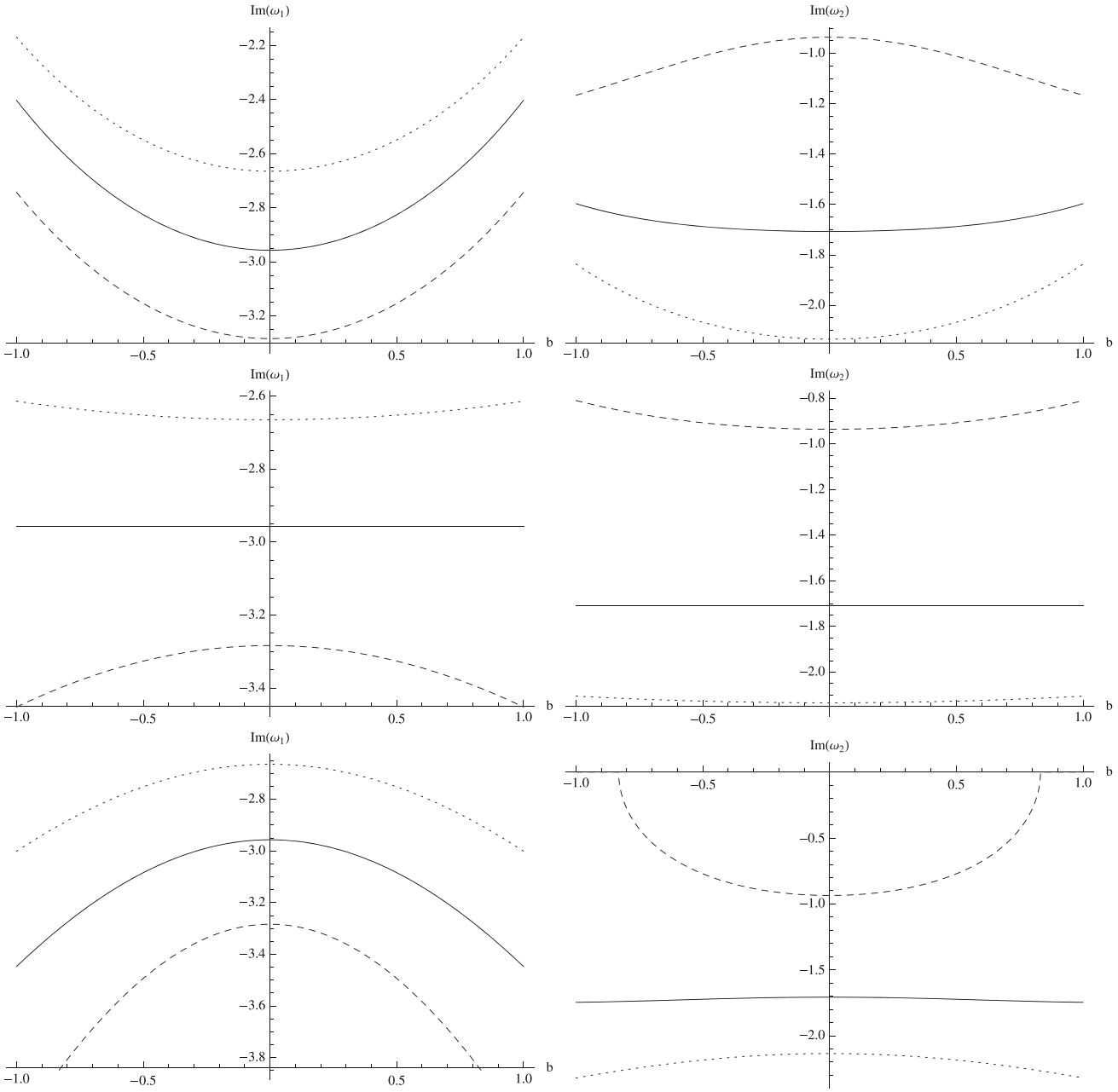

Fig. 10 The fundamental QNFs ω_1 (left) and ω_2 (right) as a function of b with $M = 1$, $a = 1$, $\Lambda = -1$, $J = 0.5$, and $m = 1$. Top panels for $\lambda = 0.8$, central panels for $\lambda = 1$, and bottom panels for $\lambda = 1.2$. Dashed lines for $\xi = 0.9$, continuous lines for $\xi = 1.0$, and dotted lines for $\xi = 1.05$

4 Remarks and conclusions

In this work, we computed the QNMs of rotating three-dimensional Hořava AdS black holes and we analyzed the effect of the breaking of the Lorentz invariance on the QNMs. We showed that depending on the parameters, the lapsus function can represent a spacetime without an event horizon, a black hole geometry with one event horizon, an extremal black hole and finally a black hole with two horizons. The QNMs have been obtained by imposing on the horizon that there are only ingoing waves, while at infinity Dirichlet boundary conditions and Neumann boundary conditions were imposed. We found that the propagation of the scalar field is stable in this background, since the imaginary part of the QNFs is negative. Also, we made a systematic study of the behavior of the QNMs and QNFs with respect to the angular momentum J and ξ one of the parameter that differentiates Hořava gravity from General Relativity which

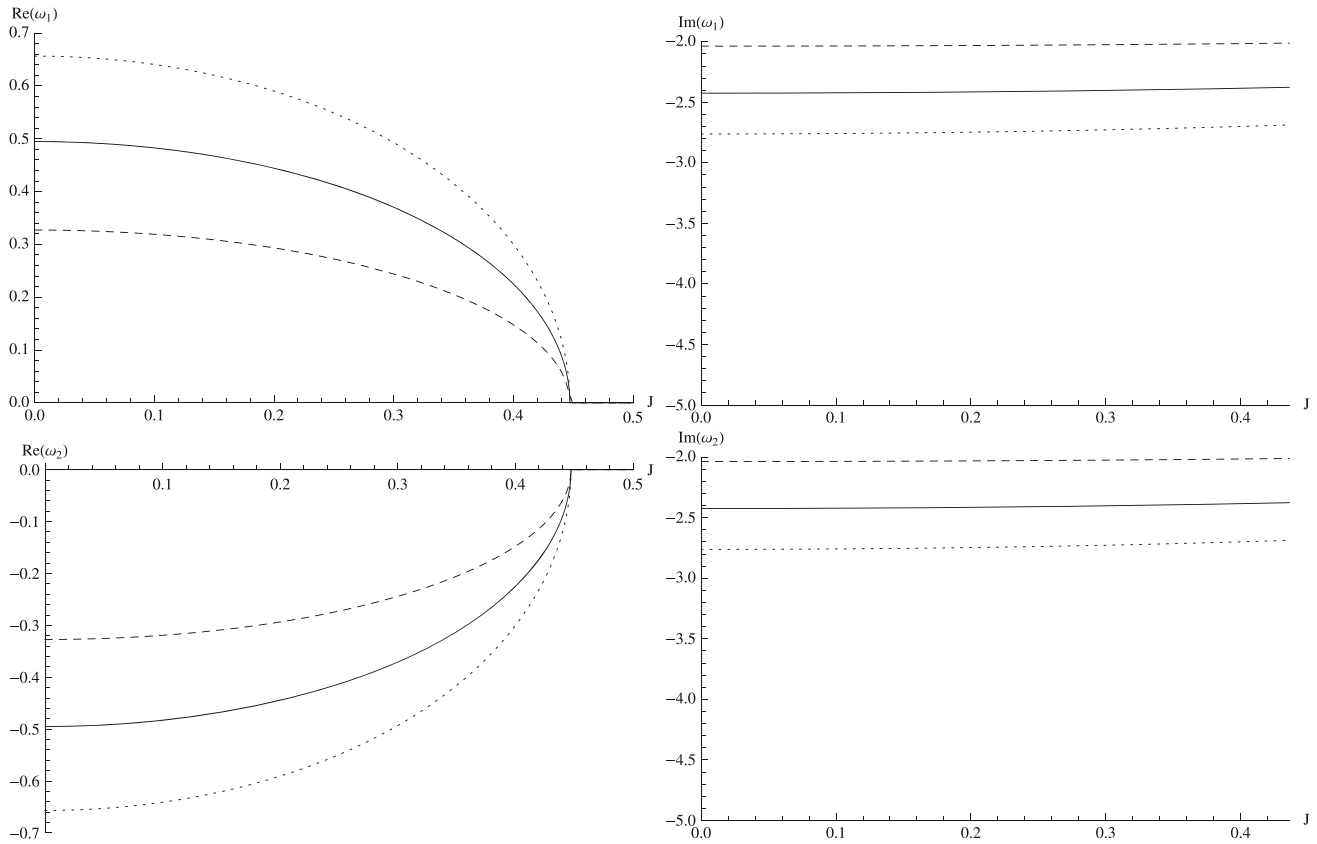

Fig. 11 The real (left) and imaginary (right) part of the fundamental quasinormal frequency (ω_1) as a function of J, for $0 < J < \sqrt{0.2}$, with $\xi = 1.05$, $M = 1$, $a = 1$, $b = 1$, $m = 1$. Dashed line for $\lambda = 0.8$, continuous line for $\lambda = 1$, and dotted line for $\lambda = 1.2$

is obtained for $\xi = 1$ and $\lambda = 1$. For various values of J and ξ, we obtained various branches of solutions with different properties of QNMs and QNFs. In particular we found the following.

For positive inner and outer horizons $r_{\pm}$, the range $\xi_e < \xi < \xi_c$ gives $Re(\omega)$ null for the fundamental QNFs, and the two sectors T_R and T_L are well defined. $|\mathrm{Im}(\omega_1)|$ increases when the parameter J increases, so according to the gauge/gravity duality, the relaxation time in order to reach the thermal equilibrium decreases. Furthermore, as the coupling constant ξ increases, $|\mathrm{Im}(\omega_1)|$ decreases and therefore the relaxation time increases. However, for ω_2, the behavior is opposite. $|\mathrm{Im}(\omega_2)|$ decreases when the parameter J increases and therefore the relaxation time increases. Furthermore, $|\mathrm{Im}(\omega_2)|$ increases when ξ increases; so, the relaxation time decreases.

In the range $\xi > \xi_c$ the black hole only has one horizon $r_+ > 0$. For this case $J^2 < 4a^2(\xi - 1)$ and the QNFs acquire a real part, with $\mathrm{Re}(\omega_1) = -\mathrm{Re}(\omega_2)$, $|\mathrm{Re}(\omega)|$ decreases when J increases, and $\mathrm{Im}(\omega_1) = \mathrm{Im}(\omega_2)$, and it is negative. Also, when ξ increases, $|\mathrm{Im}(\omega)|$ decreases. Finally, for $\xi = \xi_c$, that is, $r_- = 0$, the two sectors converge. This occurs when $J^2 + 4a^2(1 - \xi) = 0$. In this case $|\mathrm{Im}(\omega)|$ decreases when

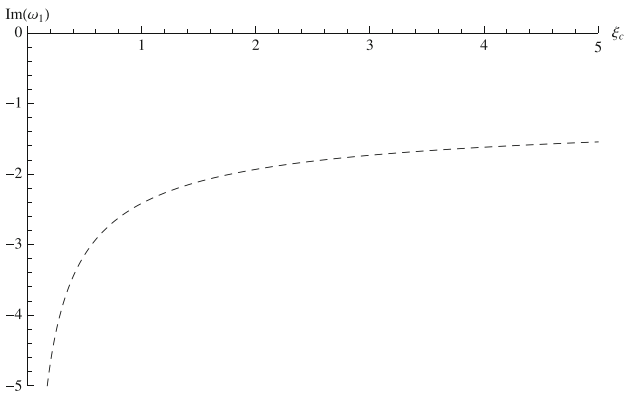

Fig. 12 The fundamental QNFs $\mathrm{Im}(\omega_1)$ as a function of ξ_c with $M = 1$, $b = 1$, $\Lambda = -1$, $\lambda = 1$, $m = 1$, and $J = 0.4$

ξ_c increases whereas $\mathrm{Re}(\omega)$ is null. Therefore, the relaxation time increases. Also, we have considered different values of the constants a and b that measure of aether misalignment, and $|\mathrm{Im}(\omega)|$ increases when the constant a or b increases; so, the relaxation time decreases.

Moreover, for the general case, that is, a massive scalar field, it was shown that the Klein–Gordon equation can be written as the Heun's differential equation, and we have stud-

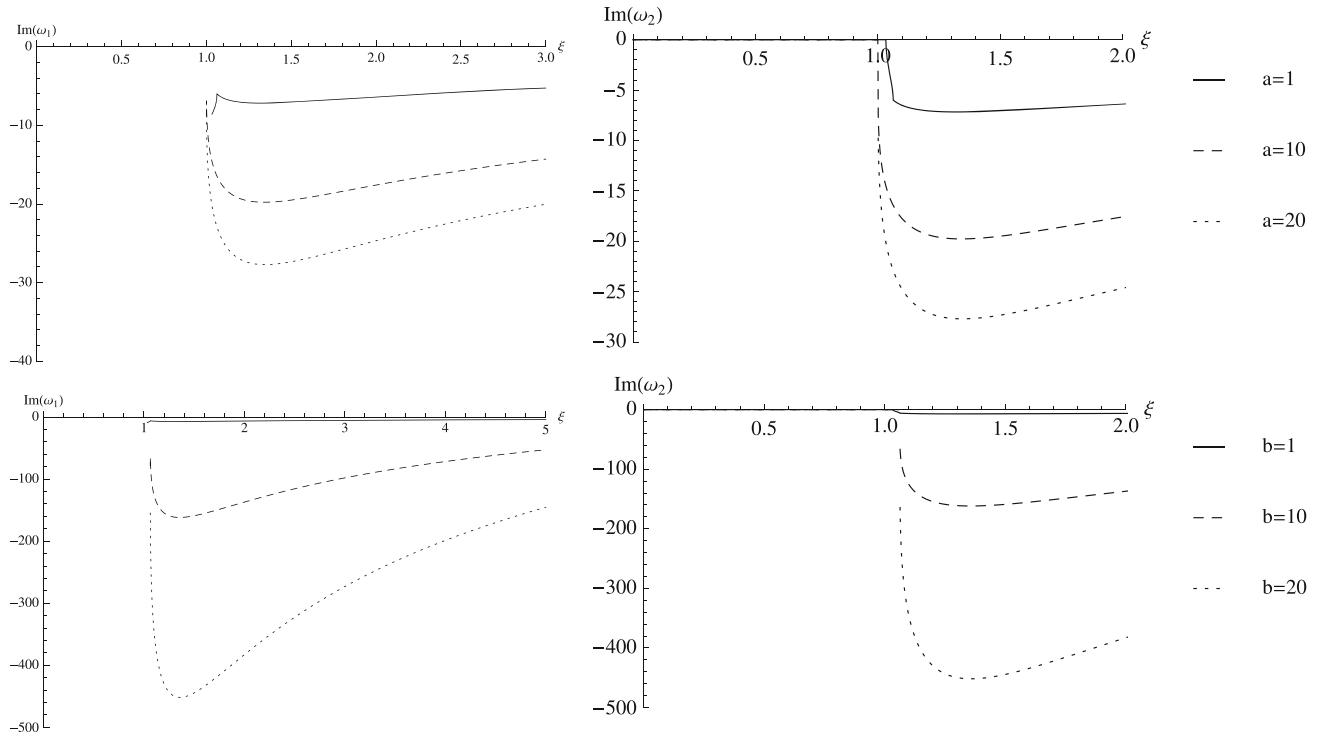

Fig. 13 The imaginary part of the fundamental QNFs ω_1 (left panels) and ω_2 (right panels) as a function of ξ, with $J = 0.5$, $M = 1$, $\Lambda = -1$, $m = 1$, and $\lambda = 5$, for different values of the constant a (top panels, with $b = 1$) and b (bottom panels, with $a = 1$)

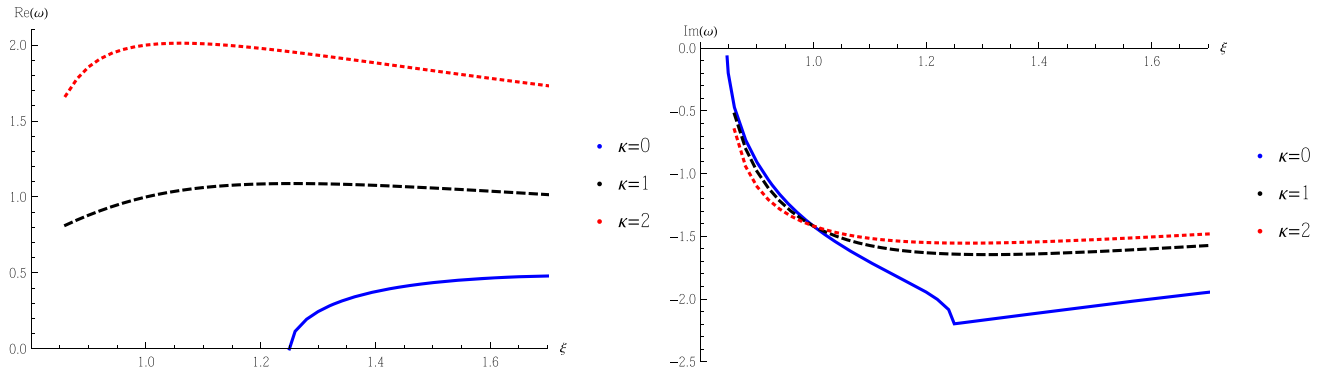

Fig. 14 The lowest QNFs for $a = 1$, $b = 1$, $\lambda = 1$, $\Lambda = -1$, $J = 1$, $m = 0.1$ and $M = 1.5$ as a function of ξ for $\kappa = 0, 1, 2$. Left panel for $\mathrm{Re}(\omega)$, and right panel for $\mathrm{Im}(\omega)$

ied the behavior of the QNMs numerically via the pseudospectral Chebyshev method, and mainly it was found that, for the lowest QNF and $\xi > 1$, the absolute value of the imaginary part decreases as κ increases; however, for $\xi < 1$ the behavior is the opposite. The absolute value of the imaginary part increases as κ increases.

As can be seen from the above discussion, the oscillatory and the decay modes of the QNMs have quite different behavior for the various branches, indicating that the time required for a system to reach thermal equilibrium on the boundary is different for the various values of the parameters. An intriguing result is that, if the parameter ξ lies between two different critical values, then the time required for the two sectors T_{R} and T_{L} to reach thermal equilibrium is competing in the sense that in one sector the time is increasing while in the other sector it is decreasing. This behavior deserves further study in connection with trying to find a system on the boundary that exhibits such a behavior.

It would be interesting to extend this work to higher dimensional Hořava black holes [57] and calculating the QNMs and QNFs of a massive wave to study how a gravity theory in the bulk with broken Lorentz invariance affects the boundary field theory to reach thermal equilibrium.

Acknowledgements Y.V. acknowledge support by the Dirección de Investigación y Desarrollo de la Universidad de La Serena, Grant No. PR18142. E.P., Y.V. and R.B would like to thank the Facultad de Ingeniería y Ciencias, Universidad Diego Portales for its hospitality, where part of this work was carried out.

Data Availability Statement This manuscript has no associated data or the data will not be deposited. [Authors' comment: This is a theoretical paper without associated data.]

Funded by SCOAP[3].

References

1. T. Regge, J.A. Wheeler, Stability of a Schwarzschild singularity. Phys. Rev. **108**, 1063 (1957)
2. F.J. Zerilli, Gravitational field of a particle falling in a schwarzschild geometry analyzed in tensor harmonics. Phys. Rev. D **2**, 2141 (1970)
3. F.J. Zerilli, Effective potential for even parity Regge-wheeler gravitational perturbation equations. Phys. Rev. Lett. **24**, 737 (1970)
4. K.D. Kokkotas, B.G. Schmidt, Quasi-normal modes of stars and black holes. Living Rev. Rel. **2**, 2 (1999). arXiv:gr-qc/9909058
5. H.P. Nollert, Topical review: quasinormal modes: the characteristic 'sound' of black holes and neutron stars. Class. Quant. Grav. **16**, R159 (1999)
6. E. Berti, V. Cardoso, A.O. Starinets, Quasinormal modes of black holes and black branes. Class. Quant. Grav. **26**, 163001 (2009). arXiv:0905.2975 [gr-qc]
7. R.A. Konoplya, A. Zhidenko, Quasinormal modes of black holes: from astrophysics to string theory. Rev. Mod. Phys. **83**, 793 (2011). arXiv:1102.4014 [gr-qc]
8. B.P. Abbott et al., [LIGO Scientific and Virgo Collaborations], Observation of Gravitational Waves from a Binary Black Hole Merger. Phys. Rev. Lett. **116**(6), 061102 (2016). arXiv:1602.03837 [gr-qc]
9. B.P. Abbott et al., [LIGO Scientific and Virgo Collaborations], Tests of general relativity with GW150914. Phys. Rev. Lett. **116**(22), 221101 (2016) (Erratum: [Phys. Rev. Lett. **121**, no. 12, 129902 (2018)]). arXiv:1602.03841 [gr-qc]
10. R. Konoplya, A. Zhidenko, Detection of gravitational waves from black holes: Is there a window for alternative theories? Phys. Lett. B **756**, 350 (2016). arXiv:1602.04738 [gr-qc]
11. A.A. Starobinsky, A new type of isotropic cosmological models without singularity. Phys. Lett. B **91**, 99 (1980)
12. A. De Felice, S. Tsujikawa, f(R) theories. Living Rev. Rel. **13**, 3 (2010). arXiv:1002.4928 [gr-qc]
13. S. Nojiri, S.D. Odintsov, Modified Gauss-Bonnet theory as gravitational alternative for dark energy. Phys. Lett. B **631**, 1 (2005). arXiv:hep-th/0508049
14. A. Nicolis, R. Rattazzi, E. Trincherini, The Galileon as a local modification of gravity. Phys. Rev. D **79**, 064036 (2009). arXiv:0811.2197
15. C. Deffayet, G. Esposito-Farese, A. Vikman, Covariant Galileon. Phys. Rev. D **79**, 084003 (2009). arXiv:0901.1314
16. T. Kolyvaris, G. Koutsoumbas, E. Papantonopoulos, G. Siopsis, Scalar hair from a derivative coupling of a scalar field to the Einstein Tensor. Class. Quant. Grav. **29**, 205011 (2012). arXiv:1111.0263 [gr-qc]
17. B. Wang, C.Y. Lin, E. Abdalla, Quasinormal modes of Reissner-Nordström anti-de Sitter black holes. Phys. Lett. B **481**, 79 (2000). arXiv:hep-th/0003295
18. B. Wang, C.Y. Lin, C. Molina, Quasinormal behavior of massless scalar field perturbation in Reissner-Nordstrom anti-de Sitter spacetimes. Phys. Rev. D **70**, 064025 (2004). arXiv:hep-th/0407024
19. E. Berti, K.D. Kokkotas, Asymptotic quasinormal modes of Reissner-Nordstrom and Kerr black holes. Phys. Rev. D **68**, 044027 (2003). arXiv:hep-th/0303029
20. R.A. Konoplya, Z. Stuchlik, A. Zhidenko, Massive nonminimally coupled scalar field in Reissner-Nordstrom spacetime: long-lived quasinormal modes and instability. Phys. Rev. D **98**(10), 104033 (2018). arXiv:1808.03346 [gr-qc]
21. E. Abdalla, B. Cuadros-Melgar, J. de Oliveira, A.B. Pavan, C.E. Pellicer, Vectorial and spinorial perturbations in Galileon black holes: quasinormal modes, quasiresonant modes, and stability. Phys. Rev. D **99**(4), 044023 (2019). arXiv:1810.01198 [gr-qc]
22. E. Abdalla, B. Cuadros-Melgar, R.D.B. Fontana, J. de Oliveira, E. Papantonopoulos, A.B. Pavan, Instability of Reissner-Nordström-AdS black hole under perturbations of a scalar field coupled to Einstein tensor. Phys. Rev. D **99**, 104065 (2019). arXiv:1903.10850 [gr-qc]
23. J.M. Maldacena, The large N limit of superconformal field theories and supergravity. Adv. Theor. Math. Phys. **2**, 231 (1998)
24. J.M. Maldacena, The large N limit of superconformal field theories and supergravity. Int. J. Theor. Phys. **38**, 1113 (1999). arXiv:hep-th/9711200
25. O. Aharony, S.S. Gubser, J.M. Maldacena, H. Ooguri, Y. Oz, Large N field theories, string theory and gravity. Phys. Rept. **323**, 183 (2000). arXiv:hep-th/9905111
26. D. Birmingham, I. Sachs, S.N. Solodukhin, Conformal field theory interpretation of black hole quasi-normal modes. Phys. Rev. Lett. **88**, 151301 (2002). arXiv:hep-th/0112055
27. G.T. Horowitz, V.E. Hubeny, Quasinormal modes of AdS black holes and the approach to thermal equilibrium. Phys. Rev. D **62**, 024027 (2000). arXiv:hep-th/9909056
28. M. Banados, C. Teitelboim, J. Zanelli, The Black hole in three-dimensional space-time. Phys. Rev. Lett. **69**, 1849 (1992). arXiv:hep-th/9204099
29. T.P. Sotiriou, I. Vega, D. Vernieri, Rotating black holes in three-dimensional Hoôava gravity. Phys. Rev. D **90**(4), 044046 (2014). arXiv:1405.3715 [gr-qc]
30. G. Siopsis, Analytic calculation of quasi-normal modes. Lect. Notes Phys. **769**, 471 (2009). arXiv:0804.2713 [hep-th]
31. K. Lin, V.H. Satheeshkumar, A. Wang, Static and rotating universal horizons and black holes in gravitational theories with broken Lorentz invariance. Phys. Rev. D **93**(12), 124025 (2016). arXiv:1603.05708 [gr-qc]
32. J.S.F. Chan, R.B. Mann, Phys. Rev. D **55**, 7546 (1997). arXiv:gr-qc/9612026
33. J.S.F. Chan, R.B. Mann, Phys. Rev. D **59**, 064025 (1999)
34. V. Cardoso, J.P.S. Lemos, Phys. Rev. D **63**, 124015 (2001)
35. R.A. Konoplya, Phys. Rev. D **70**, 047503 (2004)
36. B. Cuadros-Melgar, J. de Oliveira, C.E. Pellicer, Phys. Rev. D **85**, 024014 (2012)

37. R. Becar, P.A. Gonzalez, Y. Vasquez, Phys. Rev. D **89**(2), 023001 (2014). arXiv:1306.5974 [gr-qc]
38. M. Catalan, Y. Vasquez, Phys. Rev. D **90**(10), 104002 (2014)
39. P.A. González, A. Övgün, J. Saavedra, Y. Vásquez Gen, Rel. Grav. **50**(6), 62 (2018). arXiv:1711.01865 [gr-qc]
40. P.A. González, Y. Vásquez, R.N. Villalobos, Eur. Phys. J. C **77**(9), 579 (2017). arXiv:1704.00413 [hep-th]
41. Á. Rincón, G. Panotopoulos, Eur. Phys. J. C **78**(10), 858 (2018). arXiv:1810.08822 [gr-qc]
42. Á. Rincón, G. Panotopoulos, Phys. Rev. D **97**(2), 024027 (2018). arXiv:1801.03248 [hep-th]
43. A. Nicolis, R. Penco, F. Piazza, R. Rattazzi, Zoology of condensed matter: framids, ordinary stuff, extra-ordinary stuff. JHEP **1506**, 155 (2015). arXiv:1501.03845 [hep-th]
44. E. Papantonopoulos, From gravity to thermal gauge theories: the AdS/CFT correspondence. Lect. Notes Phys. **828**, 1 (2011)
45. R.A. Konoplya, A. Zhidenko, Perturbations and quasi-normal modes of black holes in Einstein-Aether theory. Phys. Lett. B **644**, 186 (2007). arXiv:gr-qc/0605082
46. C. Ding, Gravitational quasinormal modes of black holes in Einstein-aether theory. Nucl. Phys. B **938**, 736 (2019). arXiv:1812.07994 [gr-qc]
47. C. Ding, Quasinormal ringing of black holes in Einstein-aether theory. Phys. Rev. D **96**(10), 104021 (2017). arXiv:1707.06747 [gr-qc]
48. T.P. Sotiriou, M. Visser, S. Weinfurtner, Lower-dimensional Horava-Lifshitz gravity. Phys. Rev. D **83**, 124021 (2011). arXiv:1103.3013 [hep-th]
49. R.A. Konoplya, Phys. Lett. B **679**, 499 (2009). arXiv:0905.1523 [hep-th]
50. D. Blas, O. Pujolas, S. Sibiryakov, JHEP **0910**, 029 (2009). arXiv:0906.3046 [hep-th]
51. C. Charmousis, G. Niz, A. Padilla, P.M. Saffin, JHEP **0908**, 070 (2009). arXiv:0905.2579 [hep-th]
52. M. Abramowitz, A. Stegun, *Handbook of Mathematical functions* (Dover publications, New York, 1970)
53. J.P. Boyd, *Chebyshev and Fourier Spectral Methods*. *Dover Books on Mathematics*, 2nd edn. (Dover Publications, Mineola, 2001)
54. P.A. Gonzalez, E. Papantonopoulos, J. Saavedra, Y. Vasquez, Superradiant instability of near extremal and extremal four-dimensional charged Hairy black hole in anti-de sitter spacetime. Phys. Rev. D **95**(6), 064046 (2017). arXiv:1702.00439 [gr-qc]
55. P.A. Gonzalez, Y. Vasquez, R.N. Villalobos, Perturbative and nonperturbative fermionic quasinormal modes of Einstein-Gauss-Bonnet-AdS black holes. Phys. Rev. D **98**(6), 064030 (2018). arXiv:1807.11827 [gr-qc]
56. S.I. Finazzo, R. Rougemont, M. Zaniboni, R. Critelli, J. Noronha, Critical behavior of non-hydrodynamic quasinormal modes in a strongly coupled plasma. JHEP **1701**, 137 (2017). arXiv:1610.01519 [hep-th]
57. G. Koutsoumbas, E. Papantonopoulos, P. Pasipoularides, M. Tsoukalas, Black hole solutions in 5D Horava-Lifshitz gravity. Phys. Rev. D **81**, 124014 (2010). arXiv:1004.2289 [hep-th]